Concentration Fluctuations and Nano-Segregation in a Simplified Industrial Blend with Large Dynamic Asymmetry

Thomas Gambino,[†,‡] Numera Shafqat,[†,‡] Angel Alegría,[¶,†] Nicolas Malicki,[‡] Séverin Dronet,[‡] Aurel Radulescu,[§] Kirill Nemkovski,[§] Arantxa Arbe,[*,†] and Juan Colmenero[*,¶,†,‖]

†*Centro de Física de Materiales (CSIC, UPV/EHU) and Materials Physics Center MPC, Paseo Manuel de Lardizabal 5, E-20018 San Sebastián, Spain*

‡*Manufacture Française des Pneumatiques MICHELIN, Site de Ladoux, 23 place des Carmes Déchaux, F-63040, Clermont-Ferrand, Cedex 9, France*

¶*Departamento de Física de Materiales (UPV/EHU), Apartado 1072, E-20080 San Sebastián, Spain*

§*Jülich Centre for Neutron Science (JCNS) at Heinz Maier-Leibnitz Zentrum (MLZ), Forschungszentrum Jülich GmbH, Lichtenbergstraße 1, 85747 Garching, Germany*

‖*Donostia International Physics Center (DIPC), Paseo Manuel de Lardizabal 4, E-20018 San Sebastián, Spain*

E-mail: a.arbe@ehu.eus; juan.colmenero@ehu.eus

Abstract

Applying Small Angle Neutron Scattering (SANS) on isotopically labeled samples, we have characterized the thermally driven concentration fluctuations (TCF) –one of the main ingredients in the phenomenology of blend dynamics– in mixtures of Styrene-Butadiene Rubber (SBR) and oligomers of Polystyrene (PS) with different compositions. This system displays a large dynamic asymmetry and is thus a good model to explore the tunability of properties of interest in the rubber industry. The SANS experiments –complemented with neutron diffraction with polarization analysis– have allowed to determine the UCST-behavior of the blend and establish its phase diagram. We find a close vicinity of the spinodal and the vitrification lines for intermediate concentrations and samples rich in PS. This induces the freezing of the correlation length for TCF when decreasing the temperature and has also an impact on the reported dielectric response of these mixtures. Furthermore, we have deduced the relevant length scale for segmental relaxation from the comparison of SANS and dielectric results. The values found ($\approx$ 1.5–2 nm) are close to the Kuhn lengths of the components. The relevance of nanometric length scales in this system could also be tentatively attributed to an underlying nano-domain structure associated to seggregation of phenyl rings and main chains, supported by complementary X-ray diffraction experiments.

Introduction

Blending is a very common –and inexpensive– way to produce new materials with tuned properties, starting from already existing polymers.[1] The dynamical behavior of the mixtures produced, however, becomes rather complex. If the glass-transition temperatures of the two starting polymers are different –which is the propitious situation to access a wide range for tunability– two dynamic responses associated to each of the components can still be identified in their blends. This kind of systems are referred to as dynamically asymmetric mixtures and the observed dynamic heterogeneity is attributed to intra-molecular connectivity: since a given monomer is covalently bonded to other monomers of the same chain, a certain fraction of the 'averaging volume' –the relevant volume for segmental relaxation– is 'self-concentration' (SC). As a consequence, the mean composition experienced by this segment is biased toward its corresponding pure component. The self-concentration concept was raised as main ingredient of the phenomenology observed for polymer blends by Kornfield et al.[2,3] and incorporated in their model by Lodge and McLeish.[4] In addition to this dynamic heterogeneity, blends response is characterized by a strong broadening of the measured magnitudes (e. g. the dielectric permittivity or the mechanical relaxation) with respect to the homopolymers results. The origin of this effect is believed to rest on the thermally driven concentration fluctuations (TCF) existing in miscible blends. Their importance was first put forward by Fischer et al.[5,6] A concept implicitly involved in any model based on the SC and/or TCF ingredients is the relevant length scale for segmental relaxation. We shall call R_c the radius of the spherical correlation volume surrounding a test monomer that controls segmental relaxation. When models are applied to experimental data of blends, values of R_c of the order of 1-2 nm seem to be necessary for giving account for the dynamic heterogeneity effect mentioned above. However, models exclusively based on TCF usually demand for values of the order of 10-20 nm close to the glass transition T_g.[5,6] Estimations of the 'cooperative length scale' of segmental relaxation in polymers (see [7,8]) —which is the meaning of R_c in the TCF models— give values of the order of 1 to 3 nm close to T_g. The

combined effects of self-concentration and concentration fluctuations were simultaneously taken into account for describing the dielectric response of 'canonical' polymer blends.[9–12] The obtained correlation sizes are then comparable to the Kuhn segment length of the chains, apparently polymer-chain-specific and independent of blend partner and composition, even close to the glass transition (1–2 nm).

Formulations of materials with industrial interest may involve macromolecules with intricate repeating units, polydisperse in size/microstructure and/or internal architecture, among other factors. One key question to design materials with the desired end-use properties is whether the concepts and theoretical frameworks developed for academic blends can be applied also to describe the segmental dynamics of such 'real' systems. With these ideas in mind, we have recently carried out an investigation[13] on the dynamics of a mixture of high interest in the tire industry, since it involves Styrene-Butadiene Rubber (SBR) as one of the components. SBR –the main component of tires– is the synthetic elastomer with highest production worldwide. In the binary system explored, SBR was mixed (50/50) with polystyrene (PS). To improve miscibility, the PS was of low-molecular weight, containing 8 monomers in average. This mass is slightly above that of one Kuhn segment (7 monomers) of PS, the Kuhn length being ℓ_K^{PS}=18 Å.[14,15] Even so, its glass-transition temperature (≈280 K) was still about 70 K higher than that of the SBR component (≈213 K), qualifying thus the blend as a dynamically asymmetric mixture. In that work, dielectric spectroscopy (DS) was combined with quasielastic neutron scattering, in order to unravel the component dynamics of the mixture. It was found that, in fact, the 'academic' concepts deduced for 'canonical' blends –impact of SC and TCF– also apply in this system. In a further work on this line,[16] the possibility of exploring an extremely broad frequency/temperature range offered by DS was exploited in order to fully characterize the component dynamics of mixtures of different concentrations in terms a model involving both the concepts of SC and TFC, and elaborate a predictive approach for mechanical relaxation based on it.

The experimental works on blends invoking the importance of both TCF and SC, from

which the size of the relevant region of the segmental process has been deduced to be $\sim \ell_K$,[9–12] are mainly based on DS experiments. This technique is very powerful due to the above mentioned wide dynamic range accessible. However, a direct insight on concentration fluctuations is only directly provided by scattering techniques. Concentration fluctuations give rise to scattering at small angles for radiation with standard wavelength of the order of some Å. They can be particularly well investigated by means of neutron techniques (small angle neutron scattering, SANS) on samples where one of the components is deuterated and the other protonated. In this kind of samples, a high scattering contrast is induced between the components, enhancing the neutron scattered intensity. In this work, we make use of the previous knowledge acquired on the SBR/PS system of industrial interest[13,16] and focus our efforts on addressing the fundamental question: what is the relevant correlation volume for segmental relaxation for these blend components? Is it also in the range of the Kuhn length? We can provide a univocal answer exploiting the microscopic insight offered by SANS experiments supported by complementary neutron diffraction with polarization analysis. To enhance the neutron contrast, the blends investigated consisted of hydrogenated SBR (hSBR) and deuterated PS (dPS). Through the scattering vector (Q) dependence of the measured SANS intensity we have directly determined the correlation length ξ and amplitude of the thermally driven concentration fluctuations in mixtures of different compositions. This has allowed us, first of all, to determine the phase diagram of the mixture, qualifying it as belonging to the UCST-type. We have found that phase separation and glass-transition are simultaneously competing phenomena for samples rich in dPS. Furthermore, we compare the SANS results with those obtained from DS performed on the very same systems. In this way, we eliminate the uncertainties in the values of the relevant parameters involved in the theoretical model, potentially arising from considering systems with different microstructures or isotopic characteristics. This comparison reveals the value of R_c in a straightforward way. Even if one of the components, PS, is an oligomer of radius of gyration smaller than its Kuhn length ℓ_K, we arrive to values for the correlation size $2R_c$ of about 1.5–2 nm. These

values are close to ℓ_K of the blend components, since for the SBR used we determined $\ell_K \approx 16$Å by SANS. Thus, the hypothesis of Lodge and McLeish would also be confirmed by our results. We note however that in this particular blend system there is another ingredient that emphasizes the relevance of nanometric length scales from a structural point of view: the presence of nano-domains associated to the segregation of main chains and phenyl rings. Their existence is manifested in a 'pre-peak' in the static structure factor, as supported by X-ray diffraction results. Thus, this work supports, also in this simplified industrial system, the control of nanometric length scales on the microscopic mechanisms behind the α-relaxation.

Experimental

Samples

Protonated styrene-butadiene rubber (hSBR) was synthesized by anionic polymerization by the Michelin Company.[17] The copolymerization was initiated by BuLi in methylcyclohexane at 50°C. The deuterated polystyrene (dPS) sample was purchased from Polymer Source and synthesized by living anionic polymerization. Table 1 shows the molecular weights, glass-transition temperatures T_gs as determined by DSC [see Fig. 1(a)] and densities of the pure components used in this study. In Table 2 the compositions of their monomers and values of relevant parameters for SANS are compiled. The microstructure of SBR was (mass %): 47% 1,4-butadiene, 33% 1,2-butadiene and 20% styrene. Blends of different compositions (20, 40, 50 and 70% in weight of dPS, w_{PS}) were prepared by solution casting using Tetrahydrofuran (THF) as a solvent. Their average glass-transition temperatures are listed in Table 3.

The obtained films were carefully dried under vacuum at 350 K for 24 h to remove the solvent completely. Reference samples of the neat polymers were prepared in a similar way.

Table 1: Molecular weights, polydispersities, glass-transition temperatures and densities of the homopolymers.

Sample	$\overline{M}_n$ (g/mol)	$\overline{M}_w$ (g/mol)	$\overline{M}_w/\overline{M}_n$	T_g (K)	d (g/cm^3)
dPS	900	980	1.09	283	1.13
hSBR	22800	23500	1.03	214	0.95

Table 2: Composition, mass, volume, their average number in the chains and scattering length of the effective monomers, and scattering length densities for the two homopolymers.

Sample	Effective monomer	M_o (g/mol)	v_α (cm^3)	$\overline{N}$	b (cm)	ρ (cm^{-2})
dPS	$[C_8D_8]_{0.88}[C_8H_8]_{0.12}$	111	1.63x10^{-22}	9	96.58x10^{-13}	59.25x10^9
hSBR	$[C_8H_8]_{0.115}[C_4H_6]_{0.885}$	59.75	1.044x10^{-22}	393	6.36x10^{-13}	6.09x10^9

Table 3: Average glass-transition temperature, spinodal decomposition temperature, variance of the distribution of concentration fluctuations as deduced from DS and size of the relevant region for DS for each blend component averaged over the temperature range investigated by SANS and in the homogeneous regime.

w_{PS}	$\langle\phi_{PS}\rangle$	$\langle T_g\rangle$ (K)	T_s (K)	$\sqrt{\langle\delta\phi^2\rangle}$	$\langle 2R_c\rangle_T$ (Å)	$\langle 2R_c\rangle_{homo}$ (Å)
0.20	0.17	221	154	0.125	14.8±0.3	14.8±0.3
0.40	0.36	229	208	0.153	20.2±1.2	18.9±0.3
0.50	0.46	232	241	0.169	20.3±2.9	17.5±1.0
0.70	0.66	252	270	–	–	–

Small Angle Neutron Scattering

SANS experiments on the blends were performed on the instrument KWS-2 at the Forschungs-Neutronenquelle Heinz Maier-Leibnitz (MLZ) in Garching. Using an incident wavelength $\lambda = 5.27$ Å and three sample-detector distances (SSD): 1.15, 5.76 and 19.76 m, a Q-range between 0.003 and 0.47 Å^{-1} was covered. Here, the modulus of the scattering vector Q is defined as $Q = 4\pi\lambda^{-1}\sin(\theta/2)$, with θ the scattering angle. The samples were sandwiched between quarz plates and placed within a dedicated Cryofurnace equipped with sapphire windows. The experiments were carried out by heating the samples at 385 K , i. e., well above the effective glass transitions of both components, and collecting data in isothermal conditions at different temperatures between 385 K and the glass-transition temperature of neat

hSBR, i. e., deep in the glassy state of all the blends. The azimuthally averaged scattered intensities were obtained as function of Q. The signal from the corresponding background was measured and subtracted from the measurements. In addition, we also investigated at room temperature the chain conformation of the homopolymers in their respective bulks in order to determine the size of the chains. This was realized by using samples where 10% of the chains were isotopically labelled against a sea of macromolecules of similar characteristics regarding molecular weight and microstructure. In the case of SBR, the labelled 10% chains were protonated and the matrix deuterated; for PS, the inverse labelling was used due to scarce availability of deuterated stuff.

Diffraction with polarization analysis

Exploiting polarization analysis, experiments by the Diffuse Neutron Scattering Spectrometer (DNS)[18,19] also at MLZ allowed accessing the ratio between coherent and incoherent differential scattering cross sections of the samples. This analysis is based on the property that the neutron spin is flipped with 2/3 probability in incoherent scattering due to nuclear spin disorder, whereas no flip occurs in the case of coherent scattering.[20] With $\lambda = 4.2$ Å a Q-range from 0.2 to 4 Å^{-1} was covered. Experiments were carried out at 295 K. The raw data were corrected for detector efficiency, flipping ratio, sample container and absorption using MLZ standard programs.

X-Ray Diffraction

X-ray diffraction experiments were performed using a Rigaku PSAXS-L system located at the Centro de Física de Materiales (CSIC, UPV/EHU) in San Sebastian, Spain. The MicroMax-002+ X-ray Generator System is composed by a microfocus sealed tube source module and an integrated X-ray generator unit which produces $Cu\ K_\alpha$ transition photons of λ=1.54 Å. The Two-Dimensional Multiwire detector 2D-200X offering a 200 mm diameter active area with c.a. 200 micron resolution was placed at 25 cm from the sample. In this way we

measured diffraction patterns at RT in a Q-range from ≈ 0.1 to 1.6 Å^{-1}.

Model for Blend Dynamics and its Application to Dielectric Spectroscopy Results

The details about the model used and its application to the experimental data were presented in the previous paper,[16] where it successfully worked with blends of protonated SBR and PS of similar, but not identical, characteristics to those here studied. Therefore, new DS experiments were carried out on exactly the same samples investigated in this work. In the following, we sketch the main lines and assumptions involved in the formulation of the model used and summarize the results obtained for the present samples, addressing the interested reader to Ref.[16] for deeper details.

The model considers the combined effects of self-concentration (SC) and thermally activated concentration fluctuations (TCF). It is assumed that the TCF evolve on a much longer timescale than that of the segmental relaxation. Then, there would exist a quasi-static distribution of compositions, described by a probability distribution $g(\phi_\alpha)$, where ϕ_α is the concentration of the component $\alpha \in \{\text{PS, SBR}\}$ (note that in the following we will omit the specification of the isotopic labeling 'h' or 'd' in the nomenclature). For the sake of simplicity, $g(\phi_\alpha)$ is assumed to be a Gaussian centered around the macroscopic composition $\langle\phi_\alpha\rangle$:

$$g(\phi_\alpha) = \frac{1}{\sqrt{2\pi\langle\delta\phi^2\rangle}} \exp\left[-\frac{(\phi_\alpha - \langle\phi_\alpha\rangle)^2}{2\langle\delta\phi^2\rangle}\right]. \tag{1}$$

The variance $\langle\delta\phi^2\rangle$ is the mean-squared concentration fluctuation characterizing the TCF. The dynamics of a given polymer segment of component α is controlled by the local concentration in a region around the segment. This 'effective' composition is enhanced toward its corresponding pure component α due to self-concentration. This effect is usually accounted for introducing the self-concentration parameter ϕ^α_{self}; then:

$$\phi_{eff,\alpha} = \phi^{\alpha}_{self} + (1 - \phi^{\alpha}_{self})\phi_{\alpha}. \tag{2}$$

where ϕ_{α} is distributed as dictated by Eq. 1. The local compositions around segments are consequently also distributed, according to the Gaussian function

$$g(\phi_{eff,\alpha}) = \frac{1}{\sqrt{2\pi\langle\delta\phi^2_{eff,\alpha}\rangle}} \exp\left[-\frac{\left(\phi_{eff,\alpha} - \langle\phi_{eff,\alpha}\rangle\right)^2}{2\langle\delta\phi^2_{eff,\alpha}\rangle}\right]. \tag{3}$$

centered on a shifted mean effective concentration determined by the SC,

$$\langle\phi_{eff,\alpha}\rangle = \phi^{\alpha}_{self} + (1 - \phi^{\alpha}_{self})\langle\phi_{\alpha}\rangle \tag{4}$$

and of variance

$$\langle\delta\phi^2_{eff,\alpha}\rangle = (1 - \phi^{\alpha}_{self})^2\langle\delta\phi^2\rangle. \tag{5}$$

To deal with a reasonable number of free parameters in the application of the model, we assumed the same $\langle\delta\phi^2\rangle$ for both components. As shown in Fig. 1, the model provides a good description of the DS results on the blends investigated for concentrations rich in SBR, with w_{PS} up to 0.5. As it was found in Ref.[16] for blends of fully hydrogenated similar components, the results for mixtures with higher PS concentrations cannot be well described. It will be later shown by the SANS investigation that phase separation takes place for these samples. The values obtained for the parameters involved in the model were $\phi^{PS}_{self} = \phi^{SBR}_{self}$=0.2 (assumed to be independent of temperature and concentration), and the variances given in Table 3.

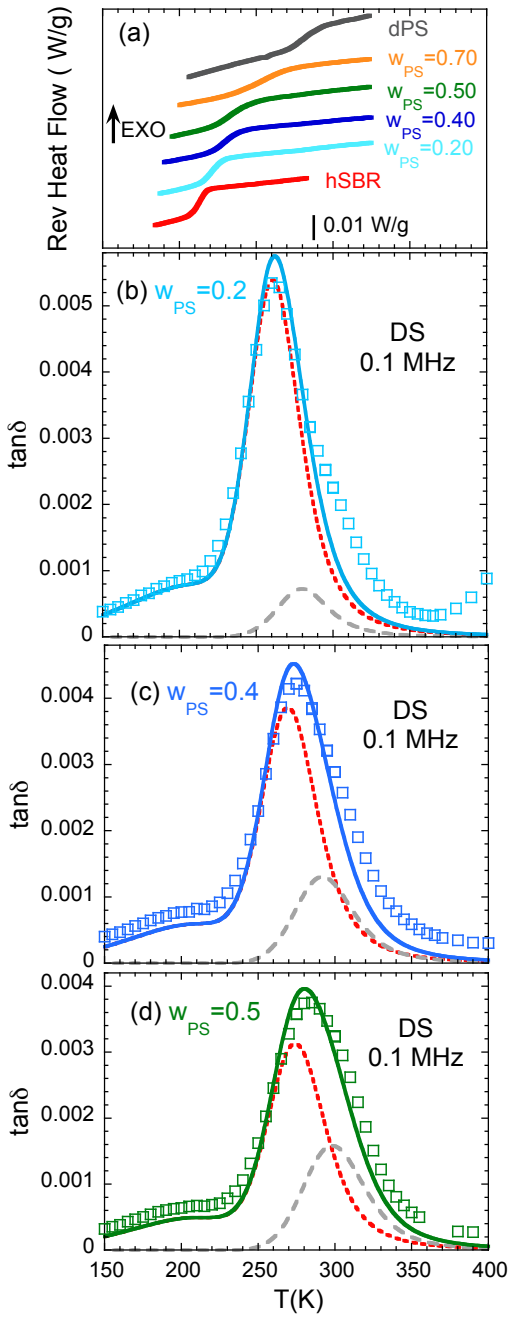

Figure 1: Panel (a) shows the calorimetry results obtained by cooling at 3K/min on the homopolymers and blends of the compositions indicated. The panels below represent broad-band dielectric spectroscopy results obtained at a frequency of 0.1MHz on blends with $w_{PS} = 0.2$ (b), 0.4 (c) and 0.5 (d) as function of temperature. Squares are experiemntal data; continuous lines are fits by the model, and the dashed and dotted lines show the contributions originated by the SBR and PS components respectively.

Results and Discussion

Structural Features of the Homopolymers

We start considering the results on the homopolymer samples. Figure 2 shows the SANS results. As a fraction of the chains is isotopically labelled, the scattered intensity arises from such contrast between the macromolecules and reflects the single chain form factor of the chain in bulk.[21] The poorer quality of the results obtained for PS is due to the small size of the macromolecules and the low signal-to-background ratio (the sample was majoritary protonated). Nevertheless, both sets of data can be reasonably well described by a Debye function accounting for the random coil conformation expected for a chain in the bulk,

$$I(Q) \;\propto\; g_D(Q) = \frac{2}{(\overline{R}_g^2 Q^2)^2}\left(e^{-\overline{R}_g^2 Q^2} - 1 + \overline{R}_g^2 Q^2\right). \qquad (6)$$

The values for $\overline{R}_g$ –the average radius of gyration of the macromolecule– obtained from the fits of Eq. 6 were 6.3 nm for SBR and about 1 nm for PS. Thus, as expected from their low molecular weight, the dimensions of the PS chains are rather small –its average end-to-end distance, $\overline{R}_e = \sqrt{6} \cdot \overline{R}_g$ ≈2 nm is similar to the reported value of ℓ_K for PS. Taking into account the microstructure of SBR, the Kuhn length obtained according to its chain dimensions from these SANS results is ℓ_K^{SBR} =15.6Å.

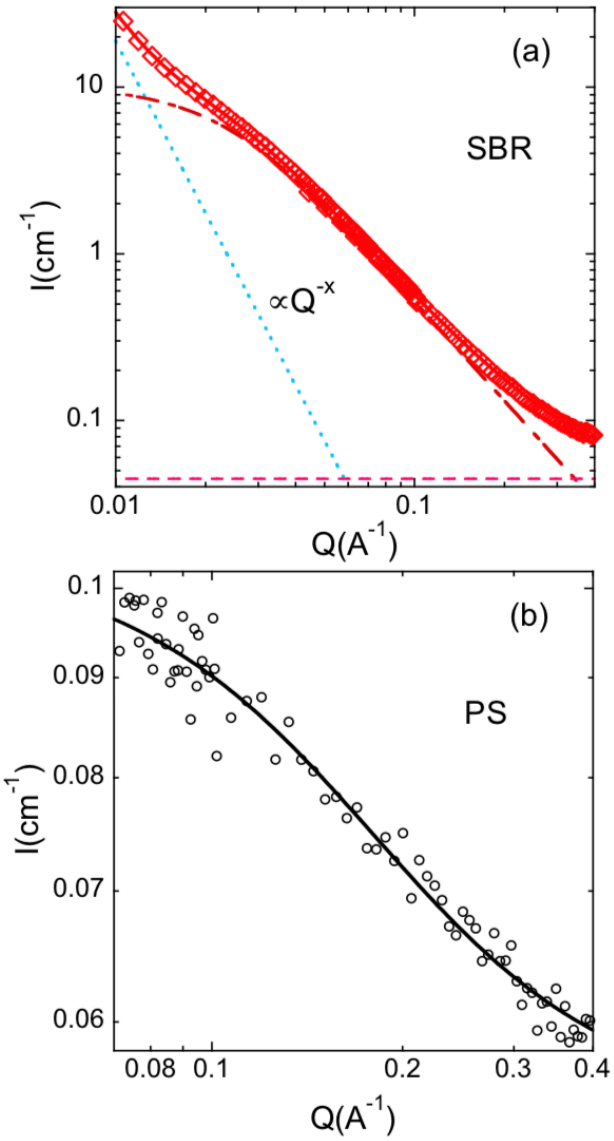

Figure 2: SANS results on homopolymer samples containing 10% labelled chains: (a) SBR melt and (b) PS melt. Lines are fits to the sum of a Debye-like form factor plus a background and, for SBR, plus a low-Q power law $I(Q) \propto Q^{-x}$, with $x = 3.4$. This kind of contribution usually arises in predominantly deuterated samples from the presence of microbubbles. The three components are separately shown in (a).

In the high-Q range, the DNS results (Fig. 3) reveal the short-range order. Since the incoherent differential cross-section does not depend on Q, the ratio between coherent and incoherent scattered intensities measured by DNS reflects the Q-dependence of coherent scattering, $I_{coh} \sim \langle \sum_{i,j} b_i b_j \exp(i\vec{Q}\vec{r}_{ij}) \rangle$ (b_i being the scattering length of nucleus i and $\vec{r}_{ij}$ the vector connecting the positions of nuclei i and j, summed over all nuclei in the sample). We note that the different isotopic composition of the samples implies that the weights of the correlations involving pairs of atoms vary from one system to another (b_C=6.65fm, b_H=-3.74fm, b_D=6.67fm). This makes the interpretation of the patterns very complicated, unless molecular dynamics (MD) simulations are used to decipher them.[22–24] The results on PS display a first pre-peak at $Q_1 \approx$0.6 Å^{-1} and a main peak at $Q_2 \approx$1.4 Å^{-1}. The existence of a pre-peak in this Q-range is common in polymers with bulky side groups and can be attributed to the nano-segregation of backbones and side-groups due to purely entropic effects.[25] In the particular case of PS, MD-simulations[26] showed that indeed rings are located close to each other in kinds of nano-domains, being $2\pi/Q_1 \approx$10 Å the distance between rings in different domains and the peak at Q_2 would mainly arise from correlations between neighboring rings (separated by $2\pi/Q_2 \approx$4.5 Å). In SBR, we find a main peak at the same position –even though for this sample, the weight of the correlations is different since it is protonated. This peak is very similar to that of pure polybutadiene[27,28] and, given the composition of our SBR [89%molar in butadiene], we shall attribute this peak to the same origin as proposed in Ref.[27] for the polybutadiene homopolymer: inter-molecular correlations from different backbones. We note the increase of the intensity in SBR at $Q <$0.6 Å^{-1} that could hint the presence of a prepeak at rather low Q-values.

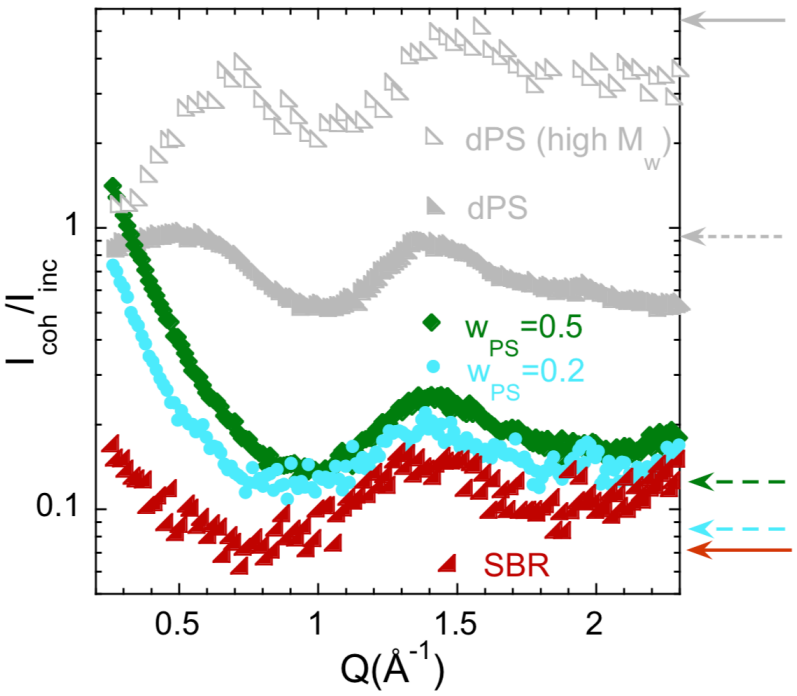

Figure 3: Ratio between the coherent and incoherent differential scattering cross section obtained from DNS experiments of diffraction with polarization analysis on the pure homopolymers investigated in this work and their blends with w_{PS}=0.2 and 0.5. Results on a high-molecular weight deuterated PS sample are also shown for comparison. The meaning of the arrows is explained in the text.

XR-diffraction experiments allowed resolving this prepeak, as can be seen in Fig. 4. It is located at $Q_1 \approx 0.35$ Å^{-1}. We recall that in the case of XR, the scattering lengths weighing the pair correlations contributions are proportional to the atomic number and the atomic form factor, and independent of isotopic labeling. We may attribute the prepeak observed in SBR to correlations between phenyl rings, which would also form nano-domains in the butadiene-like matrix. The separation between these nananodomains would then be of about $2\pi/Q_1 \approx 18$ Å.

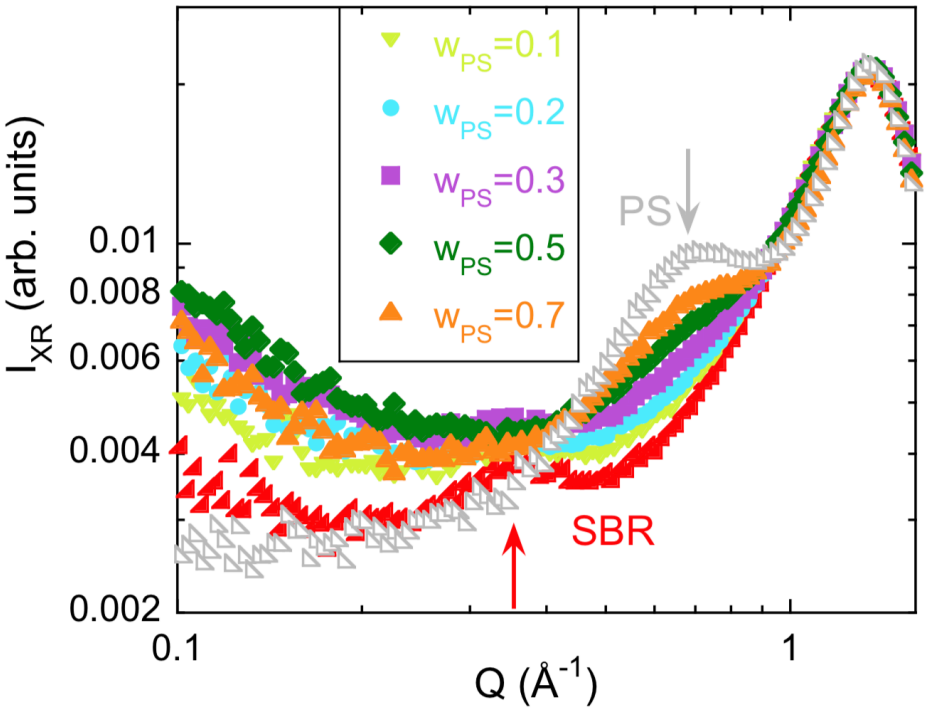

Figure 4: Small Angle X-Ray Scattering results on SBR and PS homopolymers and mixtures with different compositions. Data have been normalized to the value at the maximum of the peak centered at Q_2. The arrows mark the positions of the prepeak (Q_1) for the homopolymers.

Finally, we note that DNS reveals a deficient deuteration of the PS sample. As shown in Fig. 3, DNS results on a deuterated high-molecular weight PS sample –where the structural short-range order would presumably be the same as for our oligomeric system– display, accordingly, very similar Q-dependence. However, we find an overall scaling factor of about 6 between the two sets of data. The asymptotic $Q \to \infty$ of the measured ratio $I_{coh}(Q)/I_{inc}$ is given by the ratio between the coherent and incoherent scattering cross sections of the samples, $I_{coh}(Q \to \infty)/I_{inc} = \sigma_{coh}/\sigma_{inc}$, with $\sigma_{coh(inc)} = \sum \sigma^i_{coh(inc)}/N_{at}$ ($\sigma^i_{coh(inc)}$: coherent (incoherent) scattering cross section of atom i;[29,30] N_{at}: number of atoms in the system). The theoretical value for fully deuterated PS is indicated by the solid arrow in the figure. While the data for the high-molecular weight sample are consistent with this asymptotic value, the lower ratio in the oligomer must be attributed to the presence of some hydrogens. The experimental results would be consistent with an assumption of a deuteration level of about 88% (dotted arrow). This correction has been considered in order to calculate the values of parameters like the scattering cross sections or the scattering length density of the samples that will be used later.

Results on the Blends

The DNS results on the blends at high Q are in fact consistent with the expected asymptotic $Q \to \infty$ values calculated imposing the above estimated degree of deuteration for PS (see dashed arrows in Fig. 3). As previously commented, since in the blend samples the PS component was deuterated and SBR protonated, the interpretation of the high-Q (DNS) neutron data in terms of short-range order features is even more intrincate than in the homopolymers. Qualitatively, we can say that a prominent peak at about 1.4 Å^{-1} is still present in all samples. In the Q range where the homopolymers present a 'pre-peak', the results on the blends display a strong increase caused by the high contrast between labeled chains and reflecting concentration fluctuations that is better resolved in the SANS regime with KWS-2. Such a scattering contrast is drastically reduced for XR. As can be seen in Fig. 4, for the blends

the low-Q increase of the XR intensity is much weaker than that of neutrons. Consequently, the short-range order structural features are much better distinguished in the XR patterns. As observed for neutrons, the main feature is the peak at about 1.4 Å^{-1}. Based on the previous arguments for pure PS and SBR, it shall be attributed to nearest-neighbor chains also in the mixtures. In addition, we can also clearly distinguish a peak at about 0.7 Å^{-1} which intensity gradually decreases with increasing SBR concentration and finally becomes a shoulder on the flank of the main peak. This peak would be the signature of PS-like nano-domains persisting in the mixtures. An analogous but much weaker contribution could be envisaged in the region around 0.35 Å^{-1}, that would reflect the SBR nano-domain evolution upon addition of PS. Thus, the XR diffraction data strongly suggest the nano-segregation of phenyl rings and main-chains also in the mixtures.

Now we consider the information on thermally driven concentration fluctuations (TCF) provided by SANS. Representative SANS results for all the blend samples investigated are shown in Fig. 5. With decreasing Q, the data show a first clear increase followed by a plateau. This regime is dominated by TCF in the mixture. In the explored range of compositions, the amplitude of this contribution strongly increases with PS-concentration; for a given sample, it increases with decreasing temperature. To characterize the TCF the Ornstein-Zernike (OZ) expression is usually invoked:

$$I_{OZ}(Q) = \frac{I_{OZ}(0)}{1 + (\xi Q)^2}. \tag{7}$$

Here ξ is the correlation length and $I_{OZ}(0)$ –the $Q \to 0$ value of the function– is the amplitude for concentration fluctuations. A further steeper increase of the intensity is found below $Q \approx 0.01$ Å^{-1}, where it varies as $\propto Q^{-x}$ with $x \approx 4$. The origin of such increase of the intensity is controversial. If this Q-dependence is identified with a Porod law $\propto Q^{-4}$ arising from well-defined or 'sharp' boundaries, this intensity could be interpreted as a signature of the presence of large domains, as proposed in Ref.[31] for blends of PS and poly(vinyl

methyl ether) (PVME). For the blends of the same homopolymers, Koizumi suggested that the low-Q intensity would be describable by a Debye-Bueche function which low-Q asymptote is a Porod-like law. He attributed this regime to excess inhomogeneity resulting from stress-diffusion coupling during temperature change.[32] Conversely, the increase in intensity at low Q observed for blends of poly(ethylene oxide) (PEO) and poly(methyl methacrylate) (PMMA) was attributed to pronounced long-range density fluctuations.[33] In our case, the interpretation of this intensity is beyond the scope of our work and we will just parametrize it with a Porod-like power law. To describe the intensity measured in the whole experimental window accessed in the SANS measurements, a background (BG) has to be also added. This BG originates from incoherent contributions as well as for density fluctuations. Thus, the total expression to fit the SANS data was:

$$I_{exp}(Q) = \frac{A}{Q^x} + \frac{I_{OZ}(0)}{1 + (Q\xi)^2} + BG \tag{8}$$

with $x \equiv 4$. The values of the BG and the correlation length ξ are strongly coupled. In particular for low PS-concentrations, where the signal is weak, their univocal determination from the KWS-2 results alone becomes rather difficult due to the presence of a kind of peak at $Q \approx 0.35$ Å^{-1} –the region where the above mentioned 'pre-peak' could be expected. Therefore, the combination of SANS and DNS data can be of great help. Since SANS experiments did not involve polarization analysis, the measurements include both, coherent and incoherent contributions. Thus, to directly compare DNS and SANS data, we have obtained the total intensity from the DNS data (providing $I_{coh}(Q)/I_{inc}$) as $I_{tot}(Q) = I_{inc} + I_{coh}(Q) = I_{inc}(1 + I_{coh}(Q)/I_{inc})$. I_{inc} is the incoherent cross section per unit volume that can be calculated from the nuclear incoherent cross section values σ^i_{inc} above defined. Figure 6(a) shows representative results for a given sample and temperature. The overlap of the data is very good in the common range $Q \geq 0.13$ Å^{-1}, though the DNS results do not resolve the peak at $Q \approx 0.35$ Å^{-1}. As can be seen in this figure, the combined results are

well described by Eq. 8 with a value of BG nearly identical to the theoretical value of the incoherent intensity. Therefore, in the fit of Eq. 8 we have fixed it to the corresponding theoretical value of the incoherent contribution for each sample.

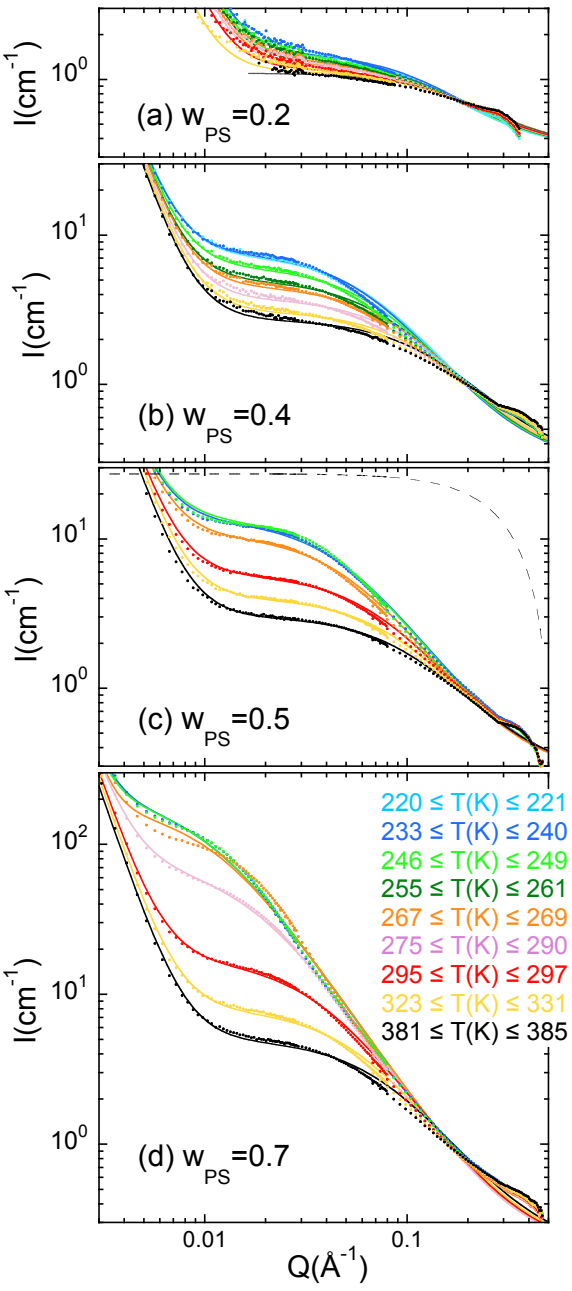

Figure 5: SANS results on the blends with PS weight fraction of 0.2 (a), 0.4 (b), 0.5 (c) and 0.7 (d). The different colors correspond to different temperatures as encoded in panel (d). The solid lines are fits of Eq. 8 to the experimental data (in the highest temperature investigated for $w_{PS} = 0.2$, the fit has been restricted to Q >0.02 Å^{-1} assuming $A = 0$). Dashed line in (c) represents, in logarithmic scale and arbitrary units, the form factor of a sphere of radius $2R_c$=17.5Å.

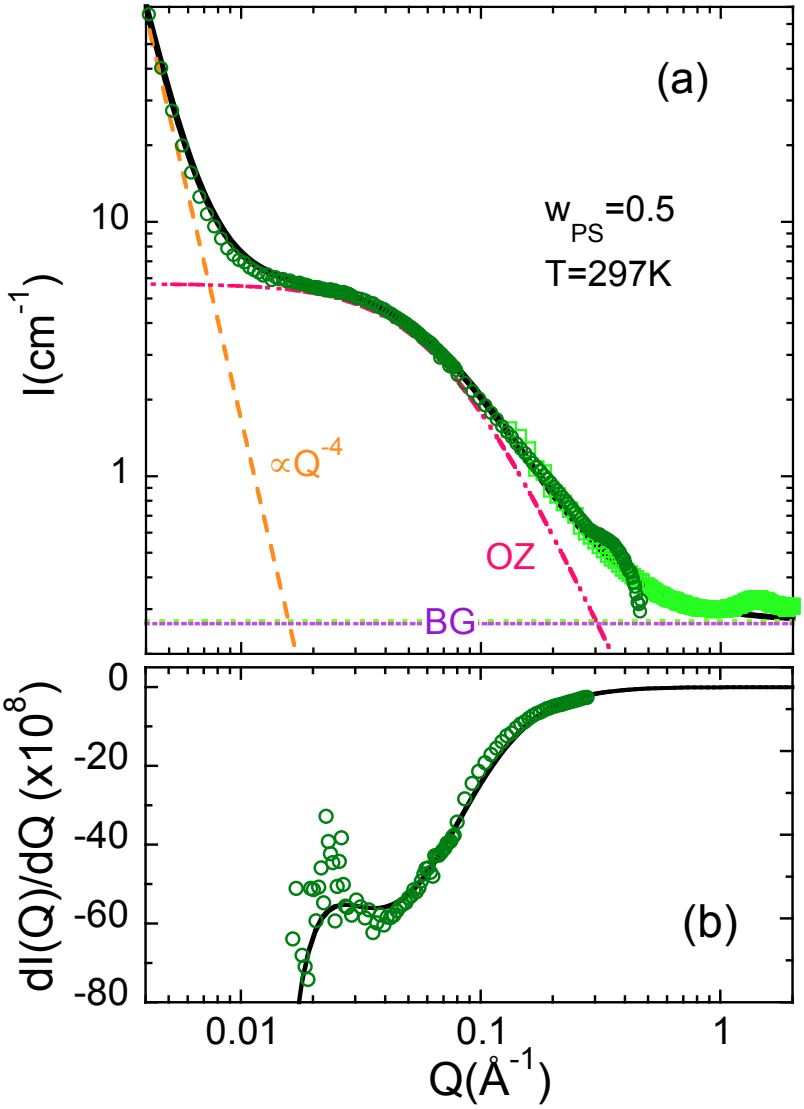

Figure 6: (a) SANS and DNS results on the sample with w_{PS}=0.5 at 297 K. Solid line is the fit of Eq. 8, with the contributions shown separately. (b) Derivative of the SANS results shown in (a) with respect to scattering vector, described by Eq. 9 (solid line).

The description of the SANS results in these terms is satisfactory, as can be appreciated in Fig. 5. The obtained values of the OZ amplitudes are represented in Fig. 7(a). This fit also gives a first estimate of the values of the characteristic lengths ξ. Except for the sample rich in PS, the such deduced values for ξ are rather small, at most of about 2 nm. As mentioned above, the BG would also contain contributions from density fluctuations. The usual estimations of these contributions based on the isothermal compressibility lead to small values, particularly when compared to the intensity of concentration fluctuations.[33–35] Conversely, as mentioned above, they have been reported to be stronger than expected in blends of PEO/PMMA.[33] Therefore, in order to obtain estimations for the ξ-values independent of the choice of the BG-value, we have considered a parallel analysis of the derivative of the SANS intensity. For this magnitude, the fitting function equivalent to Eq. 8 reads:

$$\frac{dI_{exp}(Q}{dQ} = -\frac{Ax}{Q^{(x+1)}} - \frac{2I_{OZ}(0)\xi^2 Q}{\left[1+(\xi Q)^2\right]^2}. \tag{9}$$

The derivative of the OZ function displays a minimum at $Q_{min} = 1/(\sqrt{3}\xi)$. Thus, calculating the derivative of the intensity provides a sensitive tool to determine the correlation length ξ. An example is displayed in Fig. 6(b). The values shown for ξ in Fig. 7(b) are the average of the values obtained through the two approaches. The error bars span between them.

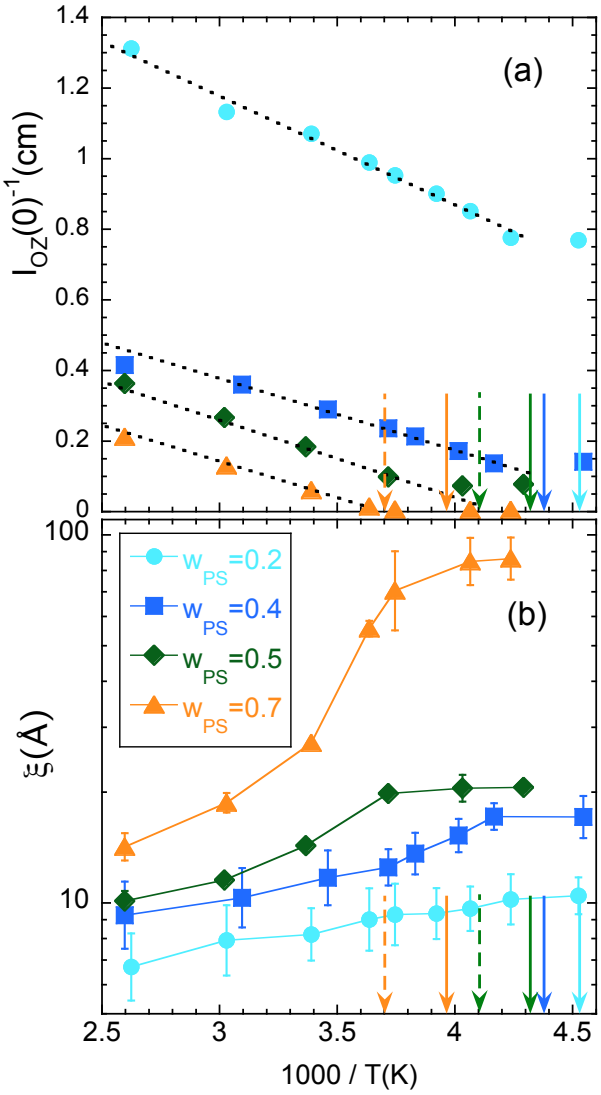

Figure 7: Inverse temperature dependence of the parameters characterizing the concentration fluctuations as deduced from SANS: inverse of the amplitude $I_{OZ}(0)$ (a) and correlation length ξ (b), for the different compositions investigated. Dotted lines in (a) show linear dependences, which extrapolations to $I_{OZ}(0)^{-1} = 0$ mark the values of the spinodal temperature T_s. They are marked by the vertical dashed arrows, while the location of the average glass-transitions determined for each sample by DSC is indicated by the continuous arrow following the same color code.

Phase Separation and Dynamic Arrest

The amplification of the concentration fluctuations with decreasing temperature points to phase separation of the mixtures at low temperatures (UCST-type phase behavior). From the temperature dependence of the parameter $I_{OZ}(0)$ representing the amplitude of these fluctuations, the spinodal decomposition temperature T_s can be determined as a function of the sample composition. The representation shown in Fig. 7(a) was applied to obtain T_s, as the value at which $I_{OZ}(0)$ tends to diverge. The resulting values are compiled in Table 3 and represented in Fig. 8(a). This figure also displays the values of the temperatures at which the behavior of $I_{OZ}(0)$ deviates from the mean field prediction $I_{OZ}(0)^{-1} \propto T^{-1}$. This temperature, denoted as T_b, could be a signature of crossing the binodal (coexisting) curve in the phase diagram.[34,36]

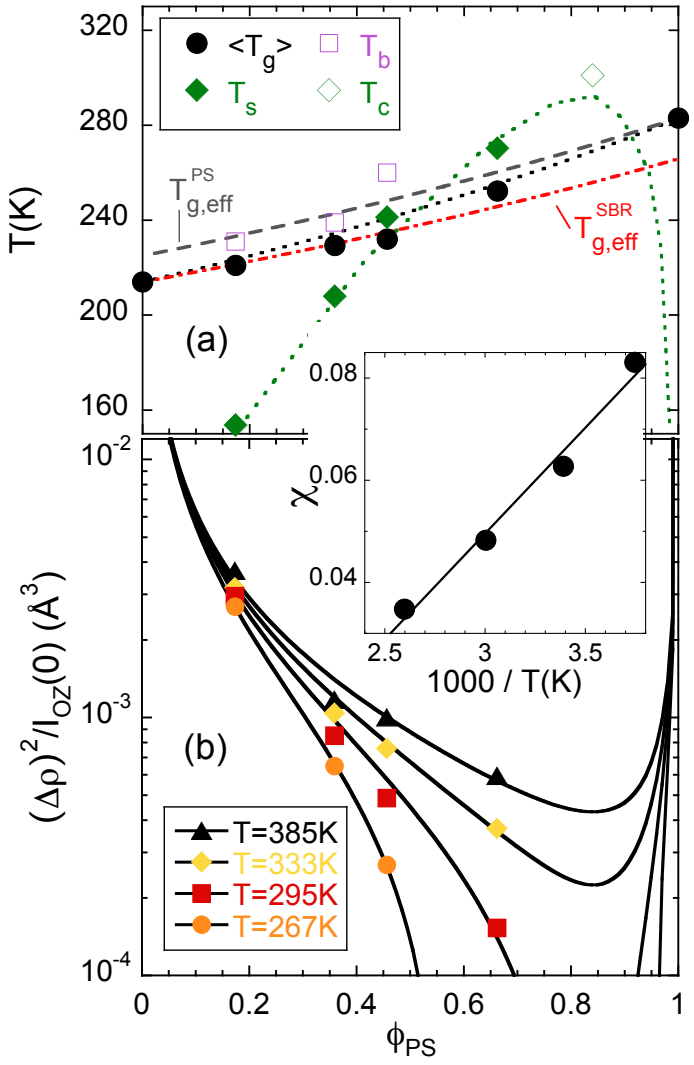

Figure 8: (a) Phase diagram showing the spinodal temperature T_s, the theoretical critical temperature T_c, the temperature T_b where the OZ amplitude deviates from the mean field behavior and the average glass-transition temperature $\langle T_g \rangle$. Dotted line connecting the homopolymer glass transitions is the Fox-Flory equation. Dashed and dashed-dotted lines represent the effective glass transition temperatures of the two blend components (see the text). Dotted line through T_s and T_c is a guide for the eyes. (b) PS-average volume fraction dependence of the inverse of $S(0)$ at the four temperatures indicated. Lines in (b) are fits to Eq. 11. The inset shows the inverse temperature dependence of the χ-parameter obtained from these fits, described by the law χ = -0.0747 + 41.45K/T.

Accompanying the amplitude of the concentration fluctuations, the associated correlation length ξ also increases with decreasing temperature, as shown in Fig. 7(b). The tendency to diverge of this parameter is only clear for the sample with highest concentration of PS. We can compare the values of ξ with the chains' dimensions, $\overline{R}_g^{SBR}$ ≈63Å, $\overline{R}_g^{PS}$ ≈10Å, assuming that they are not strongly affected by blending. ξ is smaller than both sizes (or similar to the smallest one) for the highest SBR composition, and for the highest temperatures investigated for the w_{PS}=0.4 and 0.6 samples. In such conditions, the chains are randomly mixed; otherwise, for larger correlation lengths than chain dimensions, the mixture is locally inhomogeneous.[37,38] On the other hand, we note that ξ becomes 'frozen' at the temperatures above designed as T_b.

We can invoke the mean-field theory based on the Random Phase Approximation (RPA)[39] usually applied to high-molecular polymer blends to obtain information about the interaction parameter between PS and SBR. The RPA predicts that for a binary blend of interacting polymer chains of species A and B with corresponding degrees of polymerizacion N_A and N_B, monomeric volumes v_A and v_B and average volume fractions $\langle\phi_A\rangle$ and $\langle\phi_B\rangle = 1 - \langle\phi_A\rangle$, the structure factor $S(Q)$ is given by[21,37,39]

$$\frac{1}{S(Q)} = \frac{(\Delta\rho)^2}{I(Q)} = \frac{1}{N_A\langle\phi_A\rangle v_A g_D^A(Q)} + \frac{1}{N_B(1-\langle\phi_A\rangle)v_B g_D^B(Q)} - \frac{2\chi}{v_0} \tag{10}$$

where $g_D(Q)$ is the Debye function accounting for the form factor of each of the components [Eq. 6], and v_0 is the molar volume of a reference unit cell $v_0 = \sqrt{v_A v_B}$. In Eq. 10 we have also introduced the relationship between $S(Q)$ and the intensity scattered per unit volume, $I(Q)$, through the magnitude $(\Delta\rho)^2$: the square of the difference in scattering length density ρ of the two components. In the $Q \to 0$ limit, Eq.10 results to be:

$$\frac{1}{S(0)} = \frac{(\Delta\rho)^2}{I(0)} = \frac{1}{N_A\langle\phi_A\rangle v_A} + \frac{1}{N_B(1-\langle\phi_A\rangle)v_B} - \frac{2\chi}{v_0} \tag{11}$$

The OZ function [Eq. 8] is a good approximation for Eq. 10. Thus, the previous fits of the

SANS results yield $I(0) = I_{OZ}(0)$. Using the values calculated for polymerization degrees, monomeric volumes and scattering length densities of the blend components (Table 2), Eq. 11 was thus used to describe the composition dependence of the amplitude for concentration fluctuations $I_{OZ}(0)$ for different temperatures and obtain the χ-values (see Fig. 8). In the whole temperature range investigated this parameter presents positive values, indicative for repulsive interactions between the components. Its temperature dependence can be described by the law χ = -0.0747 + 41.45K/T as shown in the inset of the figure.

Mean field theory predicts for the interaction parameter at spinodal point χ_s

$$\chi_s = \frac{v_0}{2}\left(\frac{1}{v_A N_A \phi_A} + \frac{1}{v_B N_B (1-\phi_A)}\right) \tag{12}$$

Considering the parameters of our homopolymers, the calculated critical point is $\phi_{PS,c}$=0.84 with a critical value χ_c=0.063. From the temperature dependence of χ, a value of 301 K is obtained for the critical temperature T_c. This theoretical value has been included in Fig. 8 (a). It is well compatible with the experimentally deduced values of the spinodal line.

In addition to the values of T_s and T_b deduced from the SANS experiments, Fig. 8(a) includes the average glass transition temperature $\langle T_g \rangle$ as determined by calorimetric measurements. For samples rich in SBR, $\langle T_g \rangle$ is higher than T_s: upon cooling, the sample vitrifies before demixing. The situation is opposite for high PS contents: T_s is higher than $\langle T_g \rangle$. Thus, thermodynamically the blend would tend to phase separate before it losses the equilibrium as observed by DSC. We note that there is no clear signature of a double glass-transition associated to a phase-separated system in the DSC trace [see Fig. 1(a)] for these compositions; however, as above commented, the DS results could not be properly described by the model at the highest PS concentration here considered.

As can be seen in Fig. 8(a), for samples rich in SBR, the usually invoked Fox-Flory equation $T_g^{Fox}(\langle \phi_A \rangle) = T_g^A T_g^B / [\langle \phi_A \rangle T_g^B + (1 - \langle \phi_A \rangle) T_g^A]$ fails in describing the experimentally determined $\langle T_g \rangle$. In this figure we have also included the effective glass transitions of both

components, that due to self-concentration effects differ from $\langle T_g \rangle$. We have obtained them calculating through the Fox-Flory equation the glass-transition value corresponding to the effective concentrations given by Eq. 4.[4] Apparently, for mixtures of $w_{PS} \leq 0.5$ the DSC traces manly reflect the vitrification of the SBR (low-T_g) component. A similar behavior has also been reported in another dynamically assymetric blend in Ref.[40] On the other hand, it is worth noting that for the highest SBR concentrations the temperature denoted as T_b coincides with the effective glass transition temperature of the PS component. This could point to identifying the loss of equilibrium associated to vitrification of this component as the origin of the deviations from the mean field approach observed by SANS, and not to the crossing of the binodal line. This would also be the reason of the 'freezing' of the correlation length ξ at this temperature. The other way around, approaching the binodal line could be the trigger of specific properties in this temperature range –it could namely influence e. g. the broadening of the observed calorimetric glass-transition.

Relating SANS and DS Results: Determination of the Relevant Length for Segmental Dynamics

Based on previous works of Fischer et al.,[5,6] Colby, Kumar et al.[41] proposed the following expression for the mean-squared concentration fluctuation in an incompressible binary blend:

$$\langle \delta\phi^2 \rangle = \frac{\sqrt{v_A v_B}}{4\pi^2} \int_0^\infty S(Q) Q^2 F(Q) dQ. \tag{13}$$

where $F(Q)$ is the form factor of the correlation volume. Assuming for it a sphere of radius R_c, and using the OZ approximation for the structure factor –which, as shown above, provides a very good description of the SANS data–, Eq. 13 can be expressed as:

$$\langle \delta\phi^2 \rangle = \frac{3\sqrt{v_A v_B}}{8\pi} \frac{S(0)}{R_c^3} \left\{ 1 - \frac{3(1+\check{R}_c)^2)}{2\check{R}_c^3} \left[\frac{\check{R}_c - 1}{\check{R}_c + 1} + e^{-2\check{R}_c} \right] \right\} \tag{14}$$

Here, $\check{R}_c = R_c/\xi$. Thus, the value of R_c can be obtained if we know $\langle\delta\phi^2\rangle$ from dielectric spectroscopy experiments and the values of $S(0)$ and ξ from SANS measurements.

To obtain the value of R_c for a given sample at a certain temperature, we have calculated the mean-squared concentration fluctuations expected from SANS experiments, i. e, using Eq. 14 with the values of $S(0) = I_{OZ}(0)/(\Delta\rho)^2$ and ξ from the OZ fits, as function of the variable R_c. An example is shown in Fig. 9 for the case w_{PS}=0.5 and T=385K. The value of the relevant length scale for these conditions can be directly read off from this representation, as that for which the curve assumes the value of $\langle\delta\phi^2\rangle$ obtained from the DS experiments (see Table 3). In the example here shown, R_c corresponding to $\langle\delta\phi^2\rangle$=$0.169^2$ is about 8.4Å. The values of the diameter of the sphere, $2R_c$, obtained for the three samples where the analysis of the DS results was possible are represented in Fig 10 as function of the distance from the respective average glass transition. They range between 14 and 24Å. Compared with the correlation length ξ, this magnitude shows a much weaker temperature dependence. In particular, it seems to be insensitive to temperature in the region above identified as homogeneous according to the comparison between ξ and $\overline{R}_g$ values. In this region, the values of $2R_c$ amount to 15–19Å in average (see Table 3). We may consider these values as those representative for segmental dynamics in equilibrium –free from effects associated to phase separation and/or vitrification of the blend components. The form factor of the corresponding sphere is depicted in Fig. 5(c) for illustration.

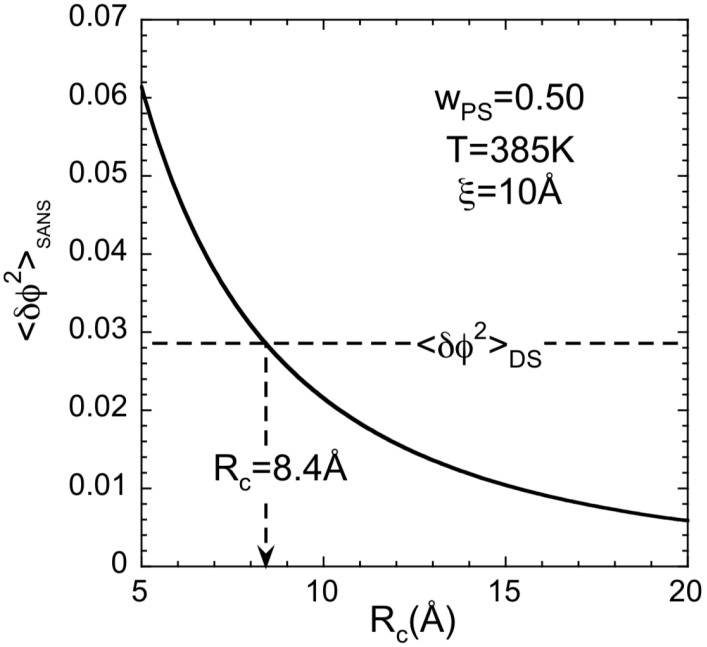

Figure 9: Mean-squared concentration fluctuation as function of the size of the relevant volume for segmental dynamics R_c, calculated according to Eq. 14 using the values found from SANS. The dashed line shows the value obtained for this magnitude from dielectric spectroscopy, and the vertical arrow marks the corresponding value for the relevant length scale.

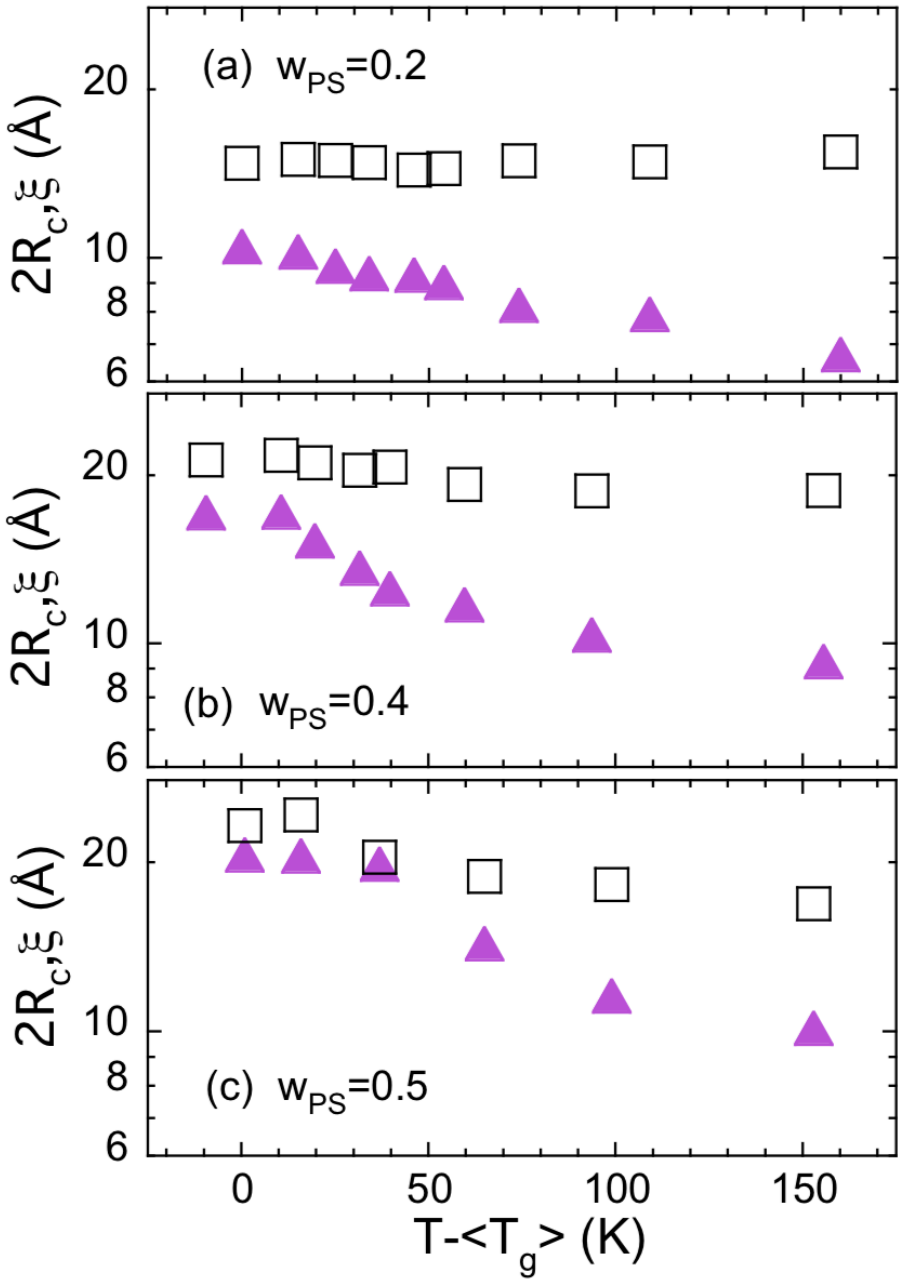

Figure 10: Temperature dependence of the diameter of the correlation sphere $2R_c$ for segmental dynamics (empty squares) and the correlation length deduced from SANS for concentration fluctuations (triangles) in the blends with PS weight fraction of 0.2 (a), 0.4 (b) and 0.5 (c).

We compare the here obtained values for $2R_c$ with those reported for components of other polymer blends from the analysis of DS results based on the same theoretical approach. They were about 8Å for 1,4-polyisoprene and poly(butylene oxide), 8–20Å for poly(vinyl ethylene), 10–12Å for PVME and 32Å for poly(2-cholorostyrene) (P2ClS) .[12] The values found here for SBR and PS are clearly larger, with exception of P2ClS. In that work, the similarity between the diameter of the spherical correlation volume and the Kuhn length of the chains was put forward. In our case, $2R_c$ is also very much comparable to ℓ_K (ℓ_K^{PS} =18Å[14,15] and ℓ_K^{SBR} =16Å). We note that in our DS-analysis we have considered a unique $\langle\delta\phi^2\rangle$-value for both components, and thereby implicitly assumed the same correlation volume for segmental relaxation in an incompressible blend. The result of a smaller value of $2R_c$ for the sample rich in SBR could be a hint that the correlation volume of the SBR component would be smaller than that of the PS component. In fact, the value obtained for the SBR-richest sample (≈1.5nm for w_{PS}=0.2) is very close to that of ℓ_K^{SBR}. Thus, our results would support again the hypothesis of Logde and McLeish[4] about the relevance of the Kuhn length in the determination of the correlation length for segmental relaxation. It is however also worthy of remark that in the particular case of the polymer blends here investigated, we could invoke another ingredient to rationalize the large values found for the correlation length of segmental relaxation: the emergence of additional structural features of nanometric size above mentioned, that give rise to the 'pre-peak' in the region 0.35-0.7Å^{-1}.

Last, we note that when the system reaches the binodal / PS-effective glass-transition temperature line, the value of the diameter of the spherical correlation volume seems to converge with the saturation value of the correlation length for concentration fluctuations ξ (see Fig. 10). Whether this is a general observation or a mere coincidence shall be subject of future work.

Summary and Conclusions

Applying SANS , neutron diffraction with polarization analysis and XR diffraction we have carried out a structural characterization of SBR and PS oligomers and their dynamically asymmetric blends. Direct access to thermally driven concentration fluctuations (TCF) has allowed to determine the interaction parameter and establish the phase diagram. The system is of UCST-type. We find a close vicinity of the spinodal and the vitrification lines for intermediate to rich in PS concentrations. Phase separation would be the reason of the observed failure of the application of the model combining self-concentration and TCF to the dielectric results on blends with high PS content. On the other hand, approaching the effective glass transition of the PS component –the slower one– in the blend would be behind the SANS observation of the freezing of the TCF amplitude and correlation length. This effect could be superimposed to crossing the binodal line for intermediate concentrations. Moreover, due to the small size of the PS component, the mixtures would be homogeneous only either at very high temperatures or for rather low PS concentrations. Under these conditions, the value deduced for the relevant length scale for segmental relaxation –deduced from the direct comparison of SANS and DS results– would be $2R_c \approx$15-22 Å. The observed increase of this magnitude with decreasing temperature approaching the glass transition at intermediate concentrations could be influenced by the approximation to phase separation. Noteworthy, the size of concentration fluctuations and relevant volume for segmental relaxation seem to converge there.

The value of $2R_c$ is close to the Kuhn lengths of the components, as proposed by Logde and McLeish. We also speculate that the underlying nano-phase separation in domains rich in phenyl rings and in main chains revealed by the scrutiny on the short-range order could impact the spatial extent for segmental dynamics of these polymers. In any case, it is worthy of remark that the control length is in the order of the nanometer scale, in good agreement with results on polymers and low-molecular glass-forming systems.[7]

Acknowledgement

We thank Robert Ngo (Michelin Advanced Research) for dSBR synthesis. The authors gratefully acknowledge the financial support of the Basque Government, code: IT-1175-19 and the Ministerio de Economía y Competitividad code: PGC2018-094548-B-I00 (MCIU/AEI/FEDER, UE). This work is based on experiments performed at KWS-2 and DNS (Heinz Maier-Leibnitz Zentrum (MLZ), Garching, Germany), and has been supported by the European Commission under the 7th Framework Programme through the 'Research Infrastructures' action of the 'Capacities' Programme, NMI3-II Grant Number 283883.

References

(1) Utracki, L., Wilkie, C., Eds. *Polymer Blends Handbook*; Springer Netherlands, 2014.

(2) Chung, G. C.; Kornfield, J. A.; Smith, S. D. Component Dynamics Miscible Polymer Blends: A Two-Dimensional Deuteron NMR Investigation. *Macromolecules* **1994**, *27*, 964–973.

(3) Chung, G.-C.; Kornfield, J. A.; Smith, S. D. Compositional Dependence of Segmental Dynamics in a Miscible Polymer Blend. *Macromolecules* **1994**, *27*, 5729–5741.

(4) Lodge, T. P.; McLeish, T. C. B. Self-Concentrations and Effective Glass Transition Temperatures in Polymer Blends. *Macromolecules* **2000**, *33*, 5278–5284.

(5) Zetsche, A.; Fischer, E. Dielectric studies of the -relaxation in miscible polymer blends and its relation to concentration fluctuations. *Acta Polymerica 45*, 168–175.

(6) Katana, G.; Fischer, E. W.; Hack, T.; Abetz, V.; Kremer, F. Influence of Concentration Fluctuations on the Dielectric .alpha.-Relaxation in Homogeneous Polymer Mixtures. *Macromolecules* **1995**, *28*, 2714–2722.

(7) Berthier, L.; Biroli, G.; Bouchaud, J.-P.; Cipelletti, L.; Masri, D. E.; L'Hôte, D.; Ladieu, F.; Pierno, M. Direct Experimental Evidence of a Growing Length Scale Accompanying the Glass Transition. *Science* **2005**, *310*, 1797–1800.

(8) Cangialosi, D.; Alegría, A.; Colmenero, J. Route to calculate the length scale for the glass transition in polymers. *Phys. Rev. E* **2007**, *76*, 011514.

(9) Leroy, E.; Alegría, A.; Colmenero, J. Segmental Dynamics in Miscible Polymer Blends: Modeling the Combined Effects of Chain Connectivity and Concentration Fluctuations. *Macromolecules* **2003**, *36*, 7280–7288.

(10) Kant, R.; Kumar, S. K.; Colby, R. H. What Length Scales Control the Dynamics of Miscible Polymer Blends? *Macromolecules* **2003**, *36*, 10087–10094.

(11) Kumar, S. K.; Shenogin, S.; Colby, R. H. Dynamics of Miscible Polymer Blends: Role of Concentration Fluctuations on Characteristic Segmental Relaxation Times. *Macromolecules* **2007**, *40*, 5759–5766.

(12) Shenogin, S.; Kant, R.; Colby, R. H.; Kumar, S. K. Dynamics of Miscible Polymer Blends: Predicting the Dielectric Response. *Macromolecules* **2007**, *40*, 5767–5775.

(13) Gambino, T.; Alegría, A.; Arbe, A.; Colmenero, J.; Malicki, N.; Dronet, S.; Schnell, B.; Lohstroh, W.; Nemkovski, K. Applying Polymer Blend Dynamics Concepts to a Simplified Industrial System. A Combined Effort by Dielectric Spectroscopy and Neutron Scattering. *Macromolecules* **2018**, *51*, 6692–6706.

(14) Rubinstein, M.; Colby, R. H. *Polymer Physics*; Oxford: Oxford University Press, 2003.

(15) Fetters, L. J.; Lohse, D. J.; Colby, R. H. In *Physical Properties of Polymers Handbook*; Mark, J. E., Ed.; Springer New York: New York, NY, 2007; pp 447–454.

(16) Gambino, T.; Alegría, A.; Arbe, A.; Colmenero, J.; Malicki, N.; Dronet, S. Modeling the

high frequency mechanical relaxation of simplified industrial polymer mixtures using dielectric relaxation results. *Polymer* **2020**, *187*, 122051.

(17) Bouty, A.; Petitjean, L.; Chatard, J.; Matmour, R.; Degrandcourt, C.; Schweins, R.; Meneau, F.; Kwasniewski, P.; Boue, F.; Couty, M.; Jestin, J. Interplay between polymer chain conformation and nanoparticle assembly in model industrial silica/rubber nanocomposites. *Faraday Discuss.* **2016**, *186*, 325–343.

(18) Su, Y.; Nemkovsiy, K.; Demirdis, S. DNS: Diffuse Scattering Neutron Tome-of-Flight Spectrometer. *Journal of Large-Scale Research Facilities JLSRF* **2015**, *1*, A27, 376–388.

(19) Schweika, W.; Böni, P. The Instrument DNS: Polarization Analysis for Diffuse Neutron Scattering. *Physica B* **2001**, *297*, 155–159.

(20) Schärpf, O. Polarization Analysis Techniques for Quasielastic Neutron Scattering. *Physica B: Condensed Matter* **1992**, *182*, 376–388.

(21) Higgins, J. S.; Benoit, H. C. *Polymers and Neutron Scattering*; Oxford University Press: Oxford, 1997.

(22) Alvarez, F.; Colmenero, J.; Zorn, R.; Willner, L.; Richter, D. Partial Structure Factors of Polyisoprene: Neutron Scattering and Molecular Dynamics Simulation. *Macromolecules* **2003**, *36*, 238–248.

(23) Genix, A.-C.; Arbe, A.; Alvarez, F.; Colmenero, J.; Schweika, W.; Richter, D. Local Structure of Syndiotactic Poly(methyl methacrylate). A Combined Study by Neutron Diffraction with Polarization Analysis and Atomistic Molecular Dynamics Simulations. *Macromolecules* **2006**, *39*, 3947–3958.

(24) Khairy, Y.; Alvarez, F.; Arbe, A.; Colmenero, J. Collective Features in Polyisobuty-

lene. A Study of the Static and Dynamic Structure Factor by Molecular Dynamics Simulations. *Macromolecules* **2014**, *47*, 447–459.

(25) Moreno, A. J.; Arbe, A.; Colmenero, J. Structure and Dynamics of Self-Assembled Comb Copolymers: Comparison between Simulations of a Generic Model and Neutron Scattering Experiments. *Macromolecules* **2011**, *44*, 1695–1706.

(26) Ayyagari, C.; Bedrov, D.; Smith, G. D. Structure of Atactic Polystyrene: A Molecular Dynamics Simulation Study. *Macromolecules* **2000**, *33*, 6194–6199.

(27) Frick, B.; Richter, D.; Ritter, C. Structural Changes near the Glass TransitionNeutron Diffraction on a Simple Polymer. *EPL (Europhysics Letters)* **1989**, *9*, 557–562.

(28) Narros, A.; Arbe, A.; Alvarez, F.; Colmenero, J.; Zorn, R.; Schweika, W.; Richter, D. Partial Structure Factors in 1,4-Polybutadiene. A Combined Neutron Scattering and Molecular Dynamics Simulations Study. *Macromolecules* **2005**, *38*, 9847–9853.

(29) Lovesey, S. W. *Theory of Neutron Scattering from Condensed Matter*; Clarendon Press: Oxford, 1984.

(30) Squires, G. L. *Introduction to thermal neutron scattering*; Cambridge university press, 1988.

(31) Schwahn, D.; Yee-Madeira, H. Spinodal Decomposition of the Polymer Blend Deuterous Polystyrene (d-PS) and Polyvinylmethylether (PVME) Studied with High Resolution Neutron Small Angle Scattering. *Colloid & Polymer Science* **1987**, *265*, 867–875.

(32) Koizumi, S. UCST Behavior Observed for a Binary Polymer Mixture of Polystyrene/Poly(vinyl methyl ether) (PS/PVME) with a PS Rich Asymmetric Composition as a Result of Dynamic Asymmetry & Imbalanced Local Stress, Viscoelastic Phase Separation, and Pinning by Vitrification. *Soft Matter* **2011**, *7*, 3984–3992.

(33) Schwahn, D.; Pipich, V.; Richter, D. Composition and Long-Range Density Fluctuations in PEO/PMMA Polymer Blends: A Result of Asymmetric Component Mobility. *Macromolecules* **2012**, *45*, 2035–2049.

(34) Mortensen, K. *Structural Studies of Polymer Systems using Small-Angle Neutron Scattering*; 2001; pp Chapter 8, pp 223–269.

(35) Mortensen, K. *Characterization of Polymer Blends*; Wiley-VCH Verlag GmbH & Co. KGaA, 2014; pp 237–268.

(36) Schwahn, D.; Mortensen, K.; Springer, T.; YeeMadeira, H.; Thomas, R. Investigation of the phase diagram and critical fluctuations of the system polyvenylmethylether and dpolystyrene with neutron small angle scattering. *The Journal of Chemical Physics* **1987**, *87*, 6078–6087.

(37) Wignall, G. D.; Melnichenko, Y. B. Recent applications of small-angle neutron scattering in strongly interacting soft condensed matter. *Reports on Progress in Physics* **2005**, *68*, 1761–1810.

(38) Yun, S. I.; Melnichenko, Y. B.; Wignall, G. D. Small-angle neutron scattering from symmetric blends of poly(dimethylsiloxane) and poly(ethylmethylsiloxane). *Polymer* **2004**, *45*, 7969 – 7977.

(39) deGennes, P. G. *Scaling Concepts in Polymer Physics*; Cornell University Press: Ithaca, NY, 1979.

(40) Harada, M.; Suzuki, T.; Ohya, M.; Kawaguchi, D.; Takano, A.; Matsushita, Y. Novel Miscible Polymer Blend of Poly(4-trimethylsilylstyrene) and Polyisoprene. *Macromolecules* **2005**, *38*, 1868–1873.

(41) Shenogin, S.; Kant, R.; Colby, R. H.; Kumar, S. K. Dynamics of Miscible Polymer Blends: Predicting the Dielectric Response. *Macromolecules* **2007**, *40*, 5767–5775.

FOR TABLE OF CONTENTS USE ONLY

'Concentration Fluctuations and Nano-Segregation in a Simplified Industrial Blend with Large Dynamic Asymmetry'

Thomas Gambino, Numera Shafqat, Angel Alegría, Nicolas Malicki, Séverin Dronet, Aurel Radulescu, Kirill Nemkovski, Arantxa Arbe and Juan Colmenero